CHAPTER 6

ROCKET MOTOR THRUST ANALYSIS WITH CFD

Assist. Prof. Dr. Feridun KARAKOÇ[1]

Fatih Enes ALP[2]

Res. Assist. Dr. Melih CANLIDİNÇ[3]

Res. Assist. Ahmet DAYANÇ[4]

DOI: https://dx.doi.org/10.5281/zenodo.8428569

[1] Assist. Prof.; Kutahya Dumlupinar University Faculty of Engineering Department of Mechanical Engineering. feridun.karakoc@dpu.edu.tr ORCID No: 0000-0002-6210-4070

[2] Student; Kutahya Dumlupinar University Faculty of Engineering Department of Mechanical Engineering. fatih.alp@ogr.dpu.edu.tr

[3] Kutahya Dumlupinar University Faculty of Engineering Department of Mechanical Engineering. melih.canlidinc@dpu.edu.tr ORCID No: 0000-0002-4011-9490

[4] Kutahya Dumlupinar University Faculty of Engineering Department of Mechanical Engineering. ahmet.dayanc@dpu.edu.tr ORCID No: 0000-0002-5214-9021

INTRODUCTION

Rockets operate based on Newton's laws of motion. Simply put, rocket engines eject high-pressure and high-temperature gases resulting from the combustion of fuel through a nozzle. The rapid expulsion of gases from the nozzle propels the rocket forward. This principle is, in fact, based on Newton's third law of motion, which states that "for every action, there is an equal and opposite reaction".

Considered a pioneer of rocket science, an American physicist and engineer Robert H. Goddard successfully launched the first liquid-fueled rocket in 1926, which is regarded as the foundation of modern rockets. This rocket is acknowledged as a step towards physical space travel and Goddard's rocket reached a speed of 60 miles per hour and a height of 12.5 meters, burning fuel for only 2.5 seconds. This rocket set the precedent for the development of multi-stage rockets and other rocket engines that would later be used in space research. Goddard later worked on both liquid fuel rocket engines and solid fuel rocket engines. He also made significant advancements in rocket fuel systems, guidance systems, and other rocket technologies (Center, 2004).

One of the most important developments in rocket engines is the V2 rocket developed by Wernher von Braun and his team at the Army Research Center in Peenemünde, Germany, during World War II (V-2 Rocket - Wikipedia, 2023). The V-2 rocket was the first long-range ballistic missile used by Nazi Germany during World War II. It is also the first vehicle that allowed a man-made object to reach space. As shown in Figure 1, this rocket used a liquid-fueled rocket engine with the capacity to reach space and is considered a precursor of ballistic missiles (Rocket - Liquid Fuel, Propulsion, Engines | Britannica, 2023). The technical specifications of the rocket can be listed as follows: length - 14 m, diameter - 1.65 m, range - 320 km, speed - 5760 km/h, altitude - 189 km, and weight - 12.5 tons.

After World War II, rocket engines continued to evolve, signaling the dawn of space exploration. The 1950s and 1960s were a period of significant advancements in rocket engine technology, especially during the "space race" between the United States and the Soviet Union.

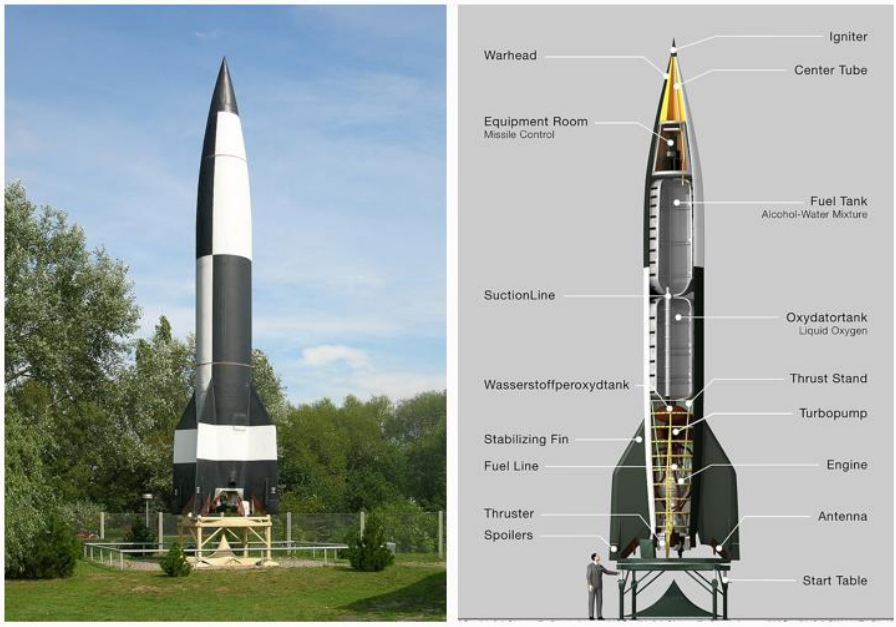

Figure 1: V-2 Rocket and Schematic View

The rocket engines developed during this time were used in the Apollo programs, as shown in Figure 2, particularly by NASA between 1961 and 1975 to carry out manned missions to the Moon (Gisler & Sornette, 2009). The Apollo spacecraft comprised a three-person cabin, a missile, and a propulsive capsule.

Figure 2: Apollo Programs

The foundation of this program, the Saturn V, as seen in Figure 3, was used to launch the first American space station, Skylab (Bilstein, 1999). Saturn V was launched 13 times from the Kennedy Space Center in Florida and has a payload capacity of 140,000 kg to low Earth orbit. This three-stage rocket used high-energy fuels such as liquid hydrogen and liquid oxygen and employed the F-1, the most powerful single-chamber liquid-fueled rocket engine ever developed, in its first stage (Young, 2008). Furthermore, as of 2021, this rocket is the only launch vehicle to have transported humans beyond low Earth orbit.

Figure 3: Saturn V Rocket

Recently, the rocket engines developed by SpaceX, as shown in Figure 4, offer significant improvements over previous generations. SpaceX is an American private space transportation company based in Hawthorne, California, founded by Elon Musk in 2002. The primary goals of the company are to reduce the cost of space transportation and establish a human colony on Mars. Chronologically, SpaceX was the first private company to reach and return a spacecraft from the International Space Station (ISS) in 2010. In 2012, the Dragon spacecraft became the first private vehicle to deliver cargo to the ISS. By 2020, SpaceX became the first private company to transport NASA astronauts to the ISS. SpaceX has developed and manufactured the

Falcon and Starship rocket families, but the Starship is designed for long-distance flights between Mars and other planets (Reddy, 2018).

Figure 4: SpaceX's Raptor Engine

SpaceX's Raptor engine provides high efficiency and reusability by using liquid methane (CH4) and liquid oxygen (O2). This engine has a "staged combustion" cycle, as shown in Figure 5, which redirects the exhaust from the gas generator back to the combustion chamber, increasing the engine's efficiency. Additionally, the Raptor engine follows the "full-flow" principle, which means that both components are completely directed to the combustion chamber, enabling the engine to produce more thrust. SpaceX uses the Raptor engine in both the Falcon rocket family and the Starship vehicle (Seedhouse, 2022).

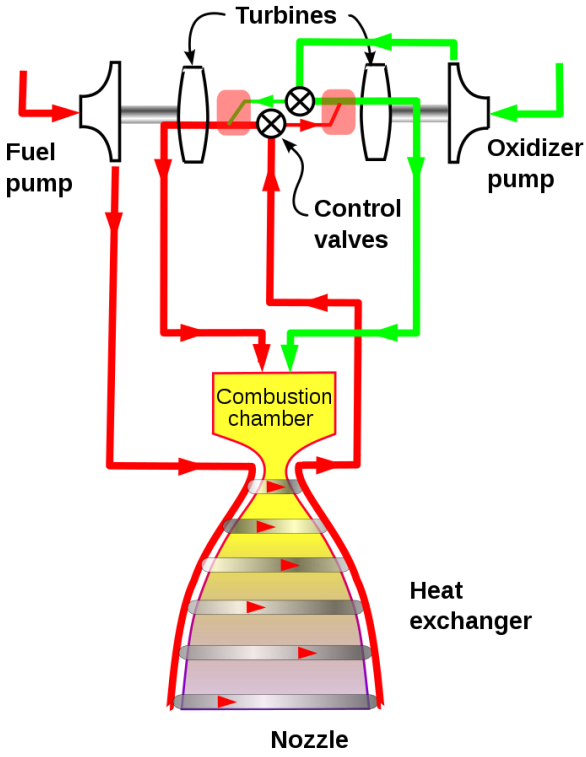

Figure 5: Full-Flow "Staged Combustion" Diagram

In our Computational Fluid Dynamics (CFD) analysis to understand the effect of the staged combustion cycle, we removed the intermediate stage where the exhaust gas is redirected back to the combustion chamber, as shown in Figure 6. Thus, we obtained less thrust force at the nozzle exit than the values explained on Nasaspaceflight, revealing how efficient the process of redirecting exhaust gas is.

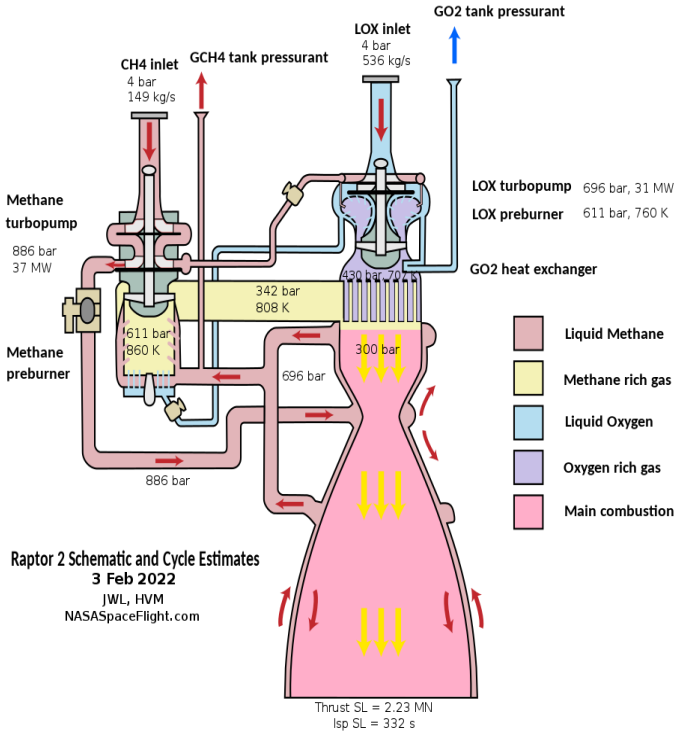

Figure 6: Raptor Engine Cycle Diagram

MATERIALS AND METHODS

For the CFD analysis, a basic CAD geometry was first drawn for the Raptor engine. In this drawing process, the dimensions were made based on the reference values of ER=35 shown in Figure 7. After the CAD geometry was created, preparations were made for the CFD analysis. The first step was to create a surface mesh from the CAD geometry. Volume mesh elements with the same edge length as the surface mesh elements were derived. Adjustments were made in the mesh parameters until mesh metrics like skewness and orthogonal geometry showed good values, and a mesh of sufficient quality to achieve mesh independence was obtained. Then, other interfaces necessary to set up the CFD analysis were opened, and the relevant parameters were defined.

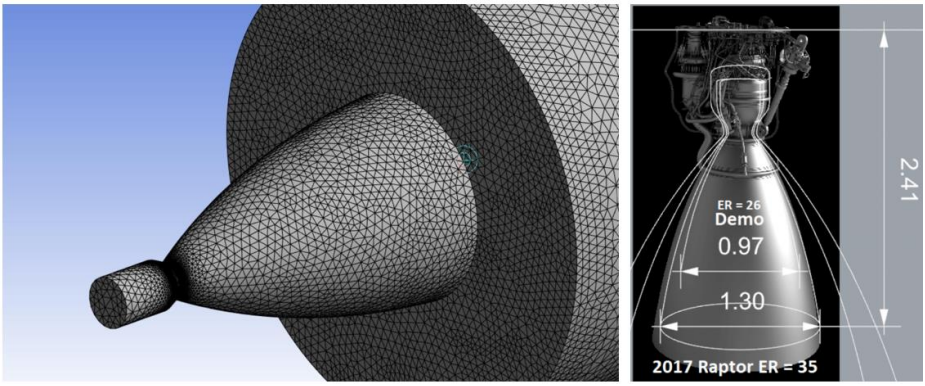

Figure 7: ER=35 Model Mesh

Input pressure and mixture ratio values were taken from NASA's CEA for combustion chamber calculations. In the interface where the material arrangement is made and seen in Figure 8, the fluid selection was made assuming an ideal gas for density properties. In addition, specific heat, molecular weight, and thermal conductivity values were entered as seen below. Due to the nature of the rocket engine, the viscosity of the fuel mixture will also not remain constant. The Viscous Sutherland Method is a method used to calculate the viscosity value of fluids in relation to temperature. Viscosity is an important property that defines the internal friction resistance of a fluid and plays a significant role in the analysis of fluid mechanics and heat transfer. Therefore, accurately estimating the viscosity of the fluid as a function of temperature is important for many applications. The advantage of the Sutherland method is that it can accurately calculate viscosity at low and high temperatures. However, at low temperatures, it would be more appropriate to use more sensitive models, especially for fluids in the liquid state. Therefore, the "Sutherland" method has been chosen to calculate the change in viscosity.

$$\mu = \mu_0 \frac{T_0+C}{T+C} \left(\frac{T}{T_0}\right)^{3/2} \quad (1)$$

In equation 1 above, μ(T) is the viscosity of the fluid at temperature T, μ_0 is the viscosity of the fluid at the reference temperature T_0, and C is a value known as the Sutherland constant (Sutherland, 1893). This method is

usually used to calculate the viscosity of gases, and for gases, the Sutherland constant is usually 110.4 K.

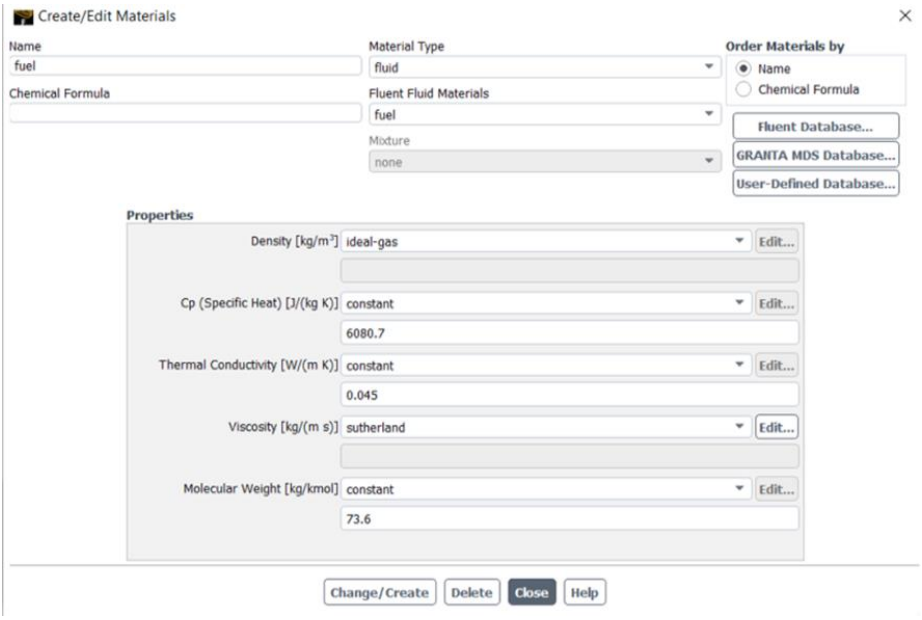

Figure 8: Properties of Material

As seen in Figure 9, since the speed of the fuel mixture is not known for the input condition, the pressure inlet parameter was defined based on the pressure at the input cross-section. After the input pressure data of 300 bar taken from NASA's CAE was defined, the supersonic initial gauge pressure value was found as a result of a calculation assuming isentropic compressed flow.

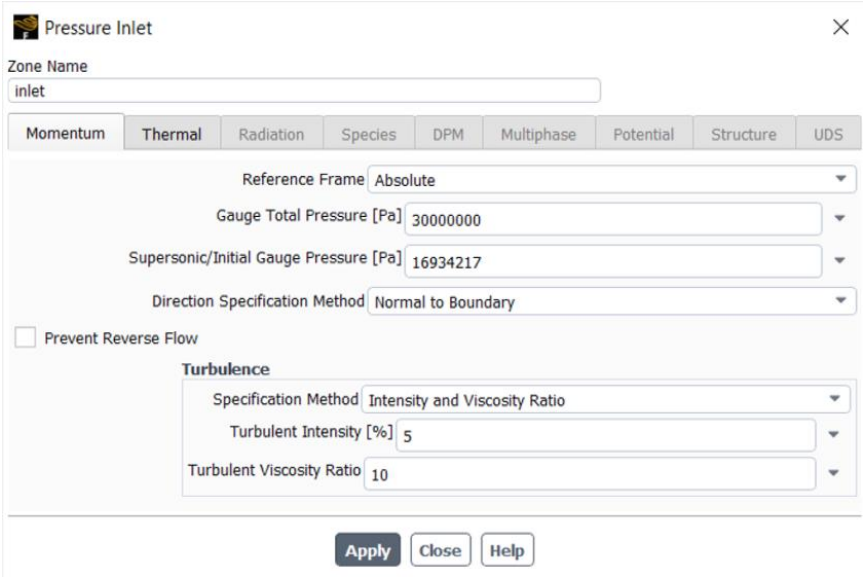

Figure 9: Definition of Inlet Boundary Condition

The scalar magnitude of the temperature input condition, which is located in the second tab of the interface related to the pressure inlet parameter shown in Figure 10, was defined as 3762.41 K in Kelvin.

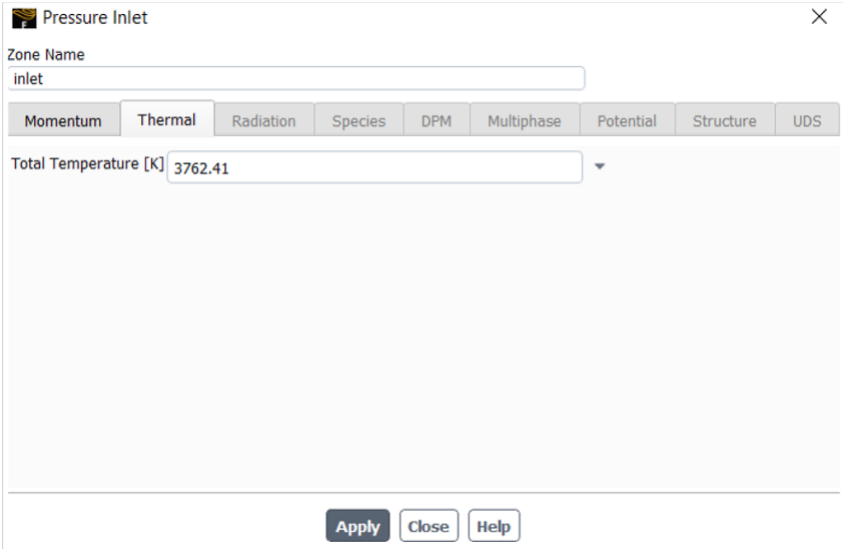

Figure 10: Defition of Inlet Temperature Condition

In the interface related to the pressure outlet parameter shown in Figure 11, there are two different tabs for momentum and thermal conditions. The value to be entered for the gauge pressure parameter in the first tab needs to be set at 101325 Pa by referring to the atmospheric pressure at sea level, as the thrust values are given as thrust sea level. In addition, the scalar magnitude of the temperature condition found in the second tab has been defined as 293 K, equivalent to 20 degrees Celsius, in correspondence with the National Institute of Standards and Technology (NIST).

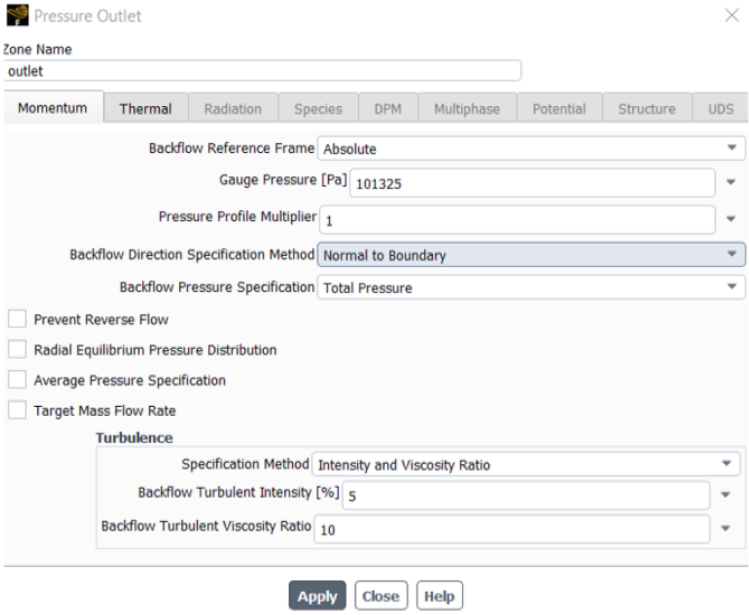

Figure 11: Definition of Outlet Boundary Condition

In the interface shown in Figure 12, a turbulence model must be selected from the list pertaining to turbulence models. The k-omega model is widely used in CFD (Computational Fluid Dynamics) analyses to calculate turbulence effects and predict the characteristics of turbulent flow.

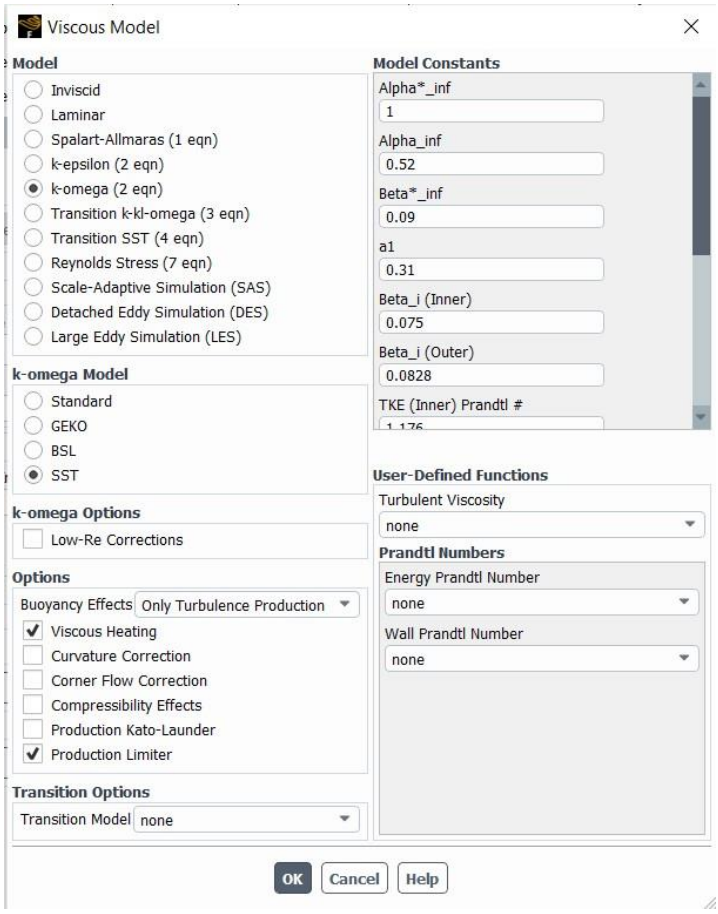

Figure 12: Setting of Viscous Model

The k-omega model uses two carrier variables named k and omega. These variables are called turbulence kinetic energy (k) and scaling frequency (omega). While turbulence kinetic energy represents the intensity of turbulent motion, the scaling frequency determines the size and interactions of turbulent structures. The k-omega model simulates turbulent flow by solving additional equations called k and omega equations, along with the Navier-Stokes equations. These additional equations are used to calculate the spreading rate of turbulence, turbulence energy production, turbulence viscosity, and other features associated with turbulence.

Such turbulence models are used to predict complex turbulent flows with less computational cost and are often preferred in industrial applications in CFD analyses. There are different variations of k-omega turbulence models used in mathematical modeling of turbulent flows.

The standard k-omega model is the basic version of the k-omega turbulence models. It is a suitable choice especially for smooth fluid flows such as high-pressure flows and circular pipes. However, it may not give sufficient results for turbulent flows involving rotational movements such as severe rotational motion and turns.

The GEKO (Generalized k-omega) model is an improved version of the k-omega model. This model is designed to more accurately predict turbulent flows where there are rotational movements and severe rotational motions. Therefore, it is a more suitable choice for rotating flows.

The BSL (Baseline) k-omega model is a variation aiming to perform better under low Reynolds numbers of turbulent flows. The Reynolds number is a parameter where the turbulence effects of the fluid become significant. The BSL model is a suitable choice to get accurate results under low Reynolds numbers.

The SST (Shear Stress Transport) k-omega model aims to achieve accurate results both near the wall surfaces and in the free flow area of turbulent flows. This model combines the advantages of k-epsilon and k-omega models and performs well across a wide flow spectrum. The SST model is a popular choice that can generally be used in various flow conditions.

Considering the suitability and effects of the differences between these variations for the rocket thrust analysis scenario and supported by the literature, the k-omega model was preferred in the choice of the turbulence model to complete the CFD analysis of the liquid-fueled rocket engine with low computational cost, and the SST variation was used in this study.

RESULTS

After all parameters were defined, the CFD analysis was run and converged in 450 iterations. In Figure 13, cross-sections of temperature results are seen. The temperature profile on the left is a section of the mixture of methane and oxygen fuel, while the temperature profile on the right shows a cross-section of the temperature profile for FLP fuel.

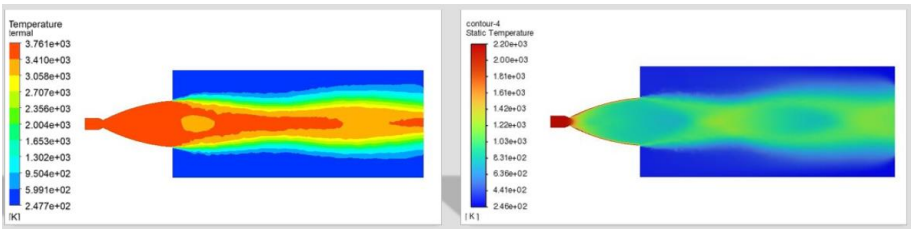

Figure 13: Temperature Profiles

In Figure 14, velocity profiles are seen. The velocity profile on the left is a section of the mixture of methane and oxygen fuel, while the velocity profile on the right shows a cross-section of the velocity profile for FLP fuel, and the velocity profile at the nozzle exit for FLP fuel turned out to be higher.

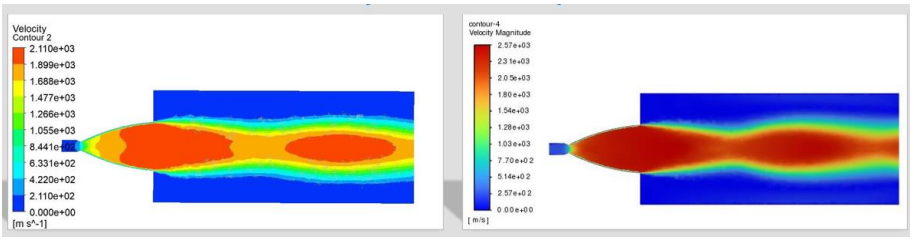

Figure 14: Speed Profiles

As a result of certain equations using the pressure, velocity, and density values obtained from the analysis, the values of mass flow rate and thrust force were found. The relevant values are given in Figure 15. It was observed that the average of the thrust force values is 1.74 MN.

X [m]	Pressure [Pa]	Velocity [m s^-	Density [kg m^-	Mass Flow	THRUST
0.00E+00	2.86E+07	2.11E+03	2.88E-01	7.89E+02	1.80E+06
1.67E-02	2.86E+07	2.11E+03	2.89E-01	790.9043355	1805552.939
3.33E-02	2.86E+07	2.11E+03	2.90E-01	793.9776119	1812156.275
5.00E-02	2.86E+07	2.11E+03	2.91E-01	797.0840412	1818920.06
6.67E-02	2.86E+07	2.11E+03	2.92E-01	800.2236434	1825846.973
8.33E-02	2.86E+07	2.11E+03	2.93E-01	803.3745521	1832759.526
1.00E-01	2.86E+07	2.11E+03	2.94E-01	806.1011453	1838917.854
1.17E-01	2.86E+07	2.11E+03	2.95E-01	808.9529904	1845561.741
1.33E-01	2.86E+07	2.11E+03	2.96E-01	811.8315589	1852289.941
1.50E-01	2.86E+07	2.11E+03	2.98E-01	816.3609831	1860505.237
1.67E-01	2.86E+07	2.11E+03	3.01E-01	824.3147108	1874613.137
1.83E-01	2.86E+07	2.11E+03	3.04E-01	832.2717854	1888904.148
2.00E-01	2.86E+07	2.10E+03	3.07E-01	840.2257889	1903154.427
2.17E-01	2.86E+07	2.10E+03	3.10E-01	846.9620617	1913344.811
2.33E-01	2.86E+07	2.10E+03	3.13E-01	854.5938365	1923116.048
2.50E-01	2.86E+07	2.10E+03	3.17E-01	865.0918484	1934016.389
2.67E-01	2.86E+07	2.10E+03	3.22E-01	876.7448853	1941311.687
2.83E-01	2.86E+07	2.09E+03	3.26E-01	888.3745315	1948447.853
3.00E-01	2.85E+07	2.09E+03	3.31E-01	900.1869823	1931498.458
3.17E-01	2.85E+07	2.09E+03	3.36E-01	913.0304594	1922446.909
3.33E-01	2.84E+07	2.08E+03	3.44E-01	931.0352225	1874979.325
3.50E-01	2.84E+07	2.08E+03	3.51E-01	948.8383089	1826880.373
3.67E-01	2.83E+07	2.08E+03	3.58E-01	966.5112222	1711323.21
3.83E-01	2.81E+07	2.07E+03	3.65E-01	984.0659397	1566750.966
4.00E-01	2.79E+07	2.07E+03	3.72E-01	1001.724825	1233541.432
4.17E-01	2.76E+07	2.07E+03	3.79E-01	1019.867662	909054.4999
4.33E-01	2.72E+07	2.07E+03	3.87E-01	1039.577565	431082.3321

Figure 15: Thrust Force Results (CH4+LOx)

In Figure 16, as a result of certain equations using the pressure, velocity, and density values obtained for FLP, the values of mass flow rate and thrust force were found. The average value of the thrust force was found to be 0.74 MN.

X [m]	Pressure [Pa]	Velocity [m s^-1]	Density [kg m^-3]	Mass Flow	THRUST
0.00E+00	2.84E+07	2.50E+03	1.98E-01	6.41E+02	8.83E+05
1.67E-02	2.84E+07	2.50E+03	1.98E-01	642.914259	886223.1635
3.33E-02	2.84E+07	2.50E+03	1.99E-01	644.10184	888694.2067
5.00E-02	2.84E+07	2.50E+03	1.99E-01	645.315951	890891.6456
6.67E-02	2.84E+07	2.50E+03	1.99E-01	646.556133	894337.6863
8.33E-02	2.84E+07	2.50E+03	2.00E-01	647.822816	897931.4163
1.00E-01	2.84E+07	2.50E+03	2.00E-01	649.124356	901268.6938
1.17E-01	2.84E+07	2.50E+03	2.00E-01	650.45811	905613.6377
1.33E-01	2.84E+07	2.50E+03	2.01E-01	651.966258	911355.2181
1.50E-01	2.84E+07	2.50E+03	2.02E-01	655.723181	921927.6718
1.67E-01	2.84E+07	2.50E+03	2.03E-01	658.995155	931228.052
1.83E-01	2.85E+07	2.50E+03	2.04E-01	662.358179	940400.6202
2.00E-01	2.85E+07	2.50E+03	2.05E-01	665.867022	948958.1119
2.17E-01	2.84E+07	2.50E+03	2.06E-01	669.389577	956431.9901
2.33E-01	2.84E+07	2.50E+03	2.07E-01	672.92533	962144.3831
2.50E-01	2.84E+07	2.50E+03	2.09E-01	677.716532	963853.1628
2.67E-01	2.84E+07	2.49E+03	2.10E-01	682.501486	964529.0496
2.83E-01	2.84E+07	2.49E+03	2.12E-01	687.281499	954513.2641
3.00E-01	2.84E+07	2.49E+03	2.14E-01	692.055188	932714.2025
3.17E-01	2.84E+07	2.49E+03	2.15E-01	696.823566	895456.3567
3.33E-01	2.83E+07	2.49E+03	2.18E-01	703.957665	841479.3441
3.50E-01	2.82E+07	2.49E+03	2.20E-01	709.825618	731836.909
3.67E-01	2.81E+07	2.48E+03	2.21E-01	714.025672	593853.5867
3.83E-01	2.79E+07	2.48E+03	2.24E-01	723.490274	384088.8535
4.00E-01	2.77E+07	2.48E+03	2.27E-01	732.936341	119670.0808

Figure 16: Thrust Force Results (FLP)

CONCLUSION

In NASA Spaceflight, the average thrust force is stated as approximately 2.23 MN for the case where the exhaust gas is redirected to the combustion chamber. In this study, when the intermediate stage in which the exhaust gas is redirected to the combustion chamber is excluded, it was observed that the average of the thrust force values dropped to 1.74 MN. Therefore, it was determined that the staged combustion cycle increases the thrust force by 25%.

One of the main reasons for working with FLP fuel is as follows: During the use of carbon-containing fuels like CH4 (methane), a large amount of carbon is released into the environment and it is clear that it damages nature, but FLP fuel does not contain carbon and have easier logistics can be a solution to this problem. However, as numerical results also show, the thrust force obtained from FLP fuel is at least half less. It was observed that the thrust force dropped from 1.74 MN to 0.74 MN. Therefore, it cannot give the capacity to free high-mass rockets from the effect of gravity and access space. It is thought that the use of FLP fuels is more suitable in smaller scale, low altitude rockets.

REFERENCES

Bilstein, R. E. (1999). Stages to Saturn: A Technological History of the Apollo/Saturn Launch Vehicle. DIANE Publishing Company.

Center, E. M. K. S. (2004). *NASA - Robert Goddard: A Man and His Rocket*.

Gisler, M., & Sornette, D. (2009). Exuberant innovations: The Apollo program. *Society*, *46*(1), 55–68. https://doi.org/10.1007/S12115-008-9163-8/FIGURES/1

Reddy, V. S. (2018). The SpaceX Effect. *Https://Home.Liebertpub.Com/Space*, *6*(2), 125–134. https://doi.org/10.1089/SPACE.2017.0032

Rocket - Liquid Fuel, Propulsion, Engines | Britannica. (2023). Retrieved August 4, 2023, from https://www.britannica.com/technology/rocket-jet-propulsion-device-and-vehicle/Liquid-propellant-rocket-engines

Seedhouse, E. (2022). The Engines. *SpaceX*, 40–57. https://doi.org/10.1007/978-3-030-99181-4_3

Sutherland, W. (1893). LII. The viscosity of gases and molecular force. *The London, Edinburgh, and Dublin Philosophical Magazine and Journal of Science*, 36(223), 507-531.

V-2 rocket - Wikipedia. (2023). Retrieved August 4, 2023, from https://en.wikipedia.org/wiki/V-2_rocket

Young, A. (2008). The Saturn V F-1 Engine. *The Saturn V F-1 Engine*. https://doi.org/10.1007/978-0-387-09630-8